Exploring amyloid formation by a *de novo* design

Richard A. Kammerer*†‡, Dirk Kostrewa†§, Jesús Zurdo†¶, Andreas Detken†‖, Carlos García-Echeverría, Janelle D. Green††, Shirley A. Müller††, Beat H. Meier‖, Fritz K. Winkler§, Christopher M. Dobson¶, and Michel O. Steinmetz‡§**

*Wellcome Trust Centre for Cell-Matrix Research, School of Biological Sciences, University of Manchester, 2205 Stopford Building, Oxford Road, Manchester M13 PT, United Kingdom; §Department of Biomolecular Research, Structural Biology Division, Paul Scherrer Insititut, CH-5232 Villigen PSI, Switzerland; ¶Department of Chemistry, University of Cambridge, Lensfield Road, Cambridge CB2 1EW, United Kingdom; ‖Department of Physical Chemistry, ETH Zurich, CH-8093 Zurich, Switzerland; **Oncology Research, Novartis Pharma AG, CH-4002 Basel, Switzerland; and ††M.E. Müller Institute for Structural Biology, Biozentrum, University of Basel, CH-4056 Basel, Switzerland

Edited by Thomas D. Pollard, Yale University, New Haven, CT, and approved January 5, 2004 (received for review October 21, 2003)

Protein deposition as amyloid fibrils underlies many debilitating human disorders. The complexity and size of disease-related polypeptides, however, often hinders a detailed rational approach to study effects that contribute to the process of amyloid formation. We report here a simplified peptide sequence successfully designed *de novo* to fold into a coiled-coil conformation under ambient conditions but to transform into amyloid fibrils at elevated temperatures. We have determined the crystal structure of the coiled-coil form and propose a detailed molecular model for the peptide in its fibrillar state. The relative stabilities of the two structural forms and the kinetics of their interconversion were found to be highly sensitive to small sequence changes. The results reveal the importance of specific packing interactions on the kinetics of amyloid formation and show the potential of this exceptionally favorable system for probing details of the molecular origins of amyloid disease.

The aggregation of soluble proteins into amyloid fibrils is the common feature of a wide variety of severely debilitating human pathologies such as Alzheimer's disease, type II diabetes, and the transmissible spongiform encephalopathies (1, 2). Recent studies suggest, moreover, that peptides and proteins possess an intrinsic ability to assemble into amyloid fibrils similar to those observed in disease states (3–5). Remarkably, despite the lack of obvious similarities among primary sequences or structure of amylogenic polypeptides, all amyloid fibrils share common characteristics such as a similar morphology, a specific β-sheet based molecular architecture, and the necessity for at least partial unfolding or proteolytic degradation of the polypeptide chain before conversion into amyloid structures (6–10).

Although substantial progress has been made in our understanding of the overall characteristics of amyloid structures and their formation, we still lack detailed knowledge of the intra- and intermolecular interactions that promote and stabilize these highly organized assemblies. Furthermore, the molecular details underlying the process of amyloid formation are still understood only in outline. These gaps in our knowledge result from the noncrystalline nature of amyloid fibrils, which makes their high-resolution structural analysis extremely challenging, and from the complexity and diversity of the different proteins that form amyloid aggregates.

To address these important issues, we have created a 17-residue peptide model system, referred to as ccβ, which forms a native-like coiled-coil structure under ambient solution conditions but which can be converted into amyloid fibrils by raising the temperature. The simplicity of the ccβ system, as well as the detailed x-ray crystal structure reported here for its coiled-coil state and the amyloid fibril model put forward on the basis of evidence from x-ray fiber diffraction, spectroscopy, and microscopy, make it highly suitable for probing molecular details of the assembly of amyloid structures.

Materials and Methods

Peptide Synthesis and Derivatization. N-acetylated and C-amidated peptides were assembled on an automated continuous-flow synthesizer, employing standard methods. Controlled oxidation of methionine residues with hydrogen peroxide was performed as described (11). The purity of the peptides was verified by reversed-phase analytical HPLC and their identities were assessed by mass spectral and amino acid analyses.

Spectroscopic Methods, Analytical Ultracentrifugation (AUC), and X-Ray Fiber Diffraction. Far UV CD spectroscopy was carried out in PBS (5 mM sodium phosphate, pH 7.4, supplemented with 150 mM NaCl) as described (12). Fourier transform infrared spectroscopy on heat-treated deuterated peptide samples obtained at p^2H 7.4 or p^2H 2.0 was performed as described (13). No significant differences in the spectra were observed between both pH values. Fibril formation was monitored by CD at 222 nm and by turbidity at 350 nm in PBS. Both methods yielded very similar results. Congo red staining of filamentous peptide samples was carried out as described (14). Sample preparation and x-ray fiber diffraction image recording by using a CuK_α rotating anode equipped with a 180- or 300-mm MAR-Research image plate were performed as described (13). AUC was performed on an Optima XL-A analytical ultracentrifuge (Beckman Instruments) equipped with an adsorption optical system (12). Sedimentation equilibrium experiments were carried out at 4°C in PBS and rotor (An-60Ti) speeds between 40,000 and 50,000 rpm. The partial specific volumes of the peptides were calculated from their amino acid sequence.

Microscopic Methods. For transmission electron microscopy (TEM), protofibrils and mature fibrils were prepared at 37°C in PBS or water (final pH 3.5). Standard negative stain specimen imaging was carried out on a Philips Morgagni TEM operated at 80 kV equipped with a Megaview III charge-coupled device camera. Mass-per-length (MPL) measurements of unstained and freeze-dried fibrils prepared in water at 37°C were carried out by using a Vacuum Generators HB-5 scanning transmission microscope (STEM), operated at 80 kV as described (15, 16). Tobacco mosaic virus (kindly supplied by R. Diaz-Avalos) served as mass standard. Atomic force microscopy (AFM) images were obtained with a Nanoscope IIIa multimode scanning probe workstation operating in tapping mode by using a silicon nitride probe with a spring constant of 0.32 N/m (17). Fibrils were prepared

This paper was submitted directly (Track II) to the PNAS office.

Abbreviations: AFM, atomic force microscopy; TEM, transmission electron microscopy; STEM, scanning TEM; AUC, analytical ultracentrifugation; REDOR, rotational-echo double-resonance; MPL, mass per length.

Data deposition: The atomic coordinates and structure factors have been deposited in the Protein Data Bank, www.rcsb.org (PDB ID code 1S9Z).

See Commentary on page 4335.

†R.A.K., D.K., J.Z., and A.D. contributed equally to this work.

‡To whom correspondence should be addressed. E-mail: richard.kammerer@man.ac.uk or michel.steinmetz@psi.ch.

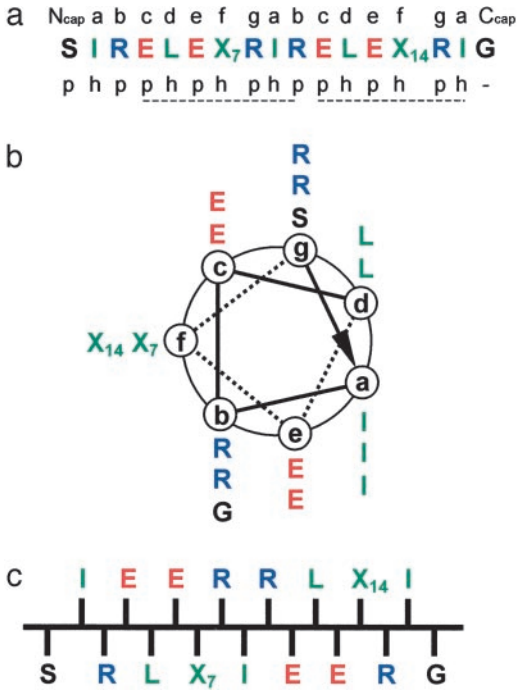

Fig. 1. Design of the ccβ model system. (*a*) Amino acid sequence of ccβ. Positions X_7 and X_{14} are occupied by Ala and Leu residues, respectively, in ccβ-p and by Met residues in ccβ-Met. The heptad repeats (**abcdefg**), capping residues (N_{cap}-acetyl and C_{cap}-amide), and the sequence patterning of polar (p) and hydrophobic (h) residues are indicated. (*b*) Helical wheel representation of ccβ as seen along the helix axis from the N terminus. (*c*) Schematic representation of ccβ in its β-strand conformation as seen along the β-sheet plane. Residues are colored according to their physicochemical properties: blue, positively charged; red, negatively charged; green, hydrophobic; black, polar and Gly.

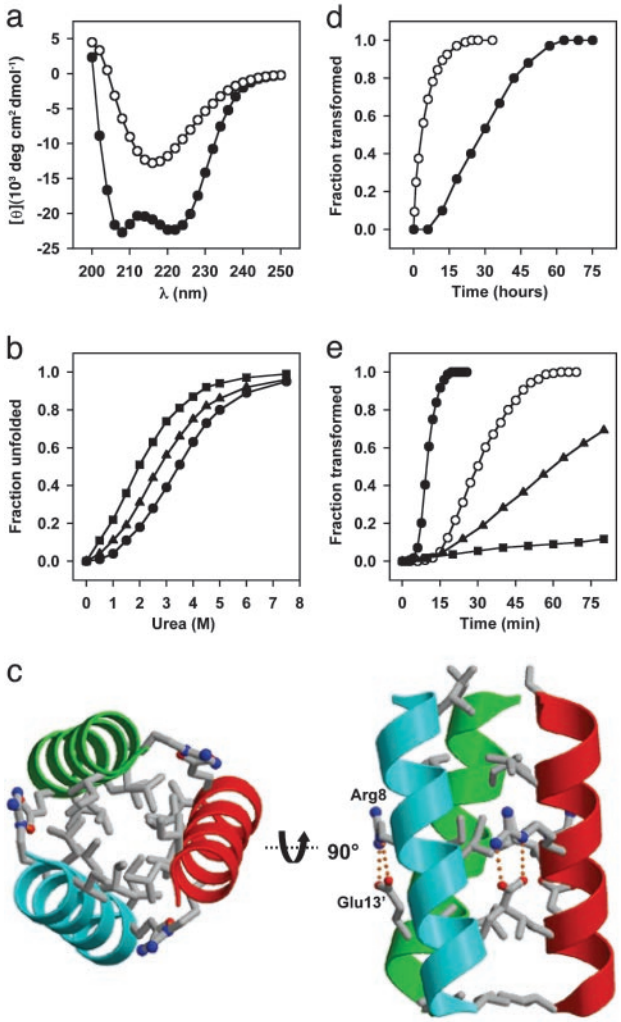

Fig. 2. Structural and kinetic analysis of ccβ variants. (*a*) CD spectra recorded from ccβ-p (0.2 mg/ml) at 4°C (●) and after incubation for 3 days at 37°C (○). (*b*) Urea-induced unfolding profiles of 0.15 mg/ml ccβ-p (●), ccβ-Met (▲), and ccβ-MetO (■) monitored by CD at 222 nm and 4°C. (*c*) A 2-Å resolution crystal structure of ccβ-p. Only the amino acid side chains at **a**, **d**, **e**, and **g** positions are shown. (*d*) α-to-β transition of ccβ-p (0.2 mg/ml) monitored at 37°C by CD at 205 nm in the absence (●) and presence (○) of 5% (wt/wt) preformed fibrils. (*e*) α-to-β transition of ccβ derivatives and peptide mixtures monitored by OD at 350 nm and 37°C: 0.4 mg/ml ccβ-Met (●), 0.2 mg/ml ccβ-Met (○), equimolar mixture of ccβ-Met and ccβ-p, 0.2 mg/ml each (▲), and equimolar mixture of ccβ-Met and ccβ-MetO, 0.2 mg/ml each (■). All spectroscopic data were obtained in PBS.

in water at 37°C and were imaged at room temperature in 10 mM Tris·HCl, pH 7.4, supplemented with 100 mM NaCl. Scan rates of 1.97 Hz and a cantilever drive frequency of ≈9 kHz were used.

Crystal Structure Determination. Hexagonal crystals were obtained overnight at 4°C by vapor diffusion using an initial peptide concentration of 5 mg/ml and a reservoir consisting of 0.05 M Na-cacodylate, pH 6.5, 0.1 M Zn-acetate, and 10% polyethylene glycol 8000. The crystals were stabilized with 30% glycerol before analysis at −180°C. An x-ray data set was collected on a MAR-Research imaging plate with a 345-mm diameter by using monochromatized CuKα radiation produced by an Enraf-Nonius FR591 rotating anode generator. The structure was solved by molecular replacement with the program CNS (18) by using a search model based on residues Ala-15-Ala-31 from the GCN4-p1 coiled-coil structure (PDB ID code 2ZTA). The final structure was obtained by iterative rounds of model building using the computer graphics program MOLOC (19) and maximum likelihood refinement program BUSTER (20). Data and refinement statistics are given in the Table 2, which is published as supporting information on the PNAS web site.

Solid-State NMR. $^{13}C\{^{15}N\}$ rotational-echo double-resonance (REDOR) experiments (21–23) were performed on a Chemagnetics Infinity 300 spectrometer operating at a magnetic field of 7.05 T, equipped with a 4-mm triple-resonance magic-angle sample spinning probe, with parameters as follows: magic-angle sample spinning frequency 6 kHz, ^{13}C radio frequency field amplitude of 50 kHz, ^{15}N radio frequency amplitude of 40 kHz, ^{1}H decoupling at an amplitude of 110 kHz. The pulse sequence of Anderson *et al.* (24) was used. Between 512 and 2,048 transients per data point were taken on a water-washed and N_2-dried ≈30 mg of fibril sample prepared in 200 mM sodium phosphate, pH 7.2, at 37°C. For the measurements the sample was cooled to −80°C. Simulated dephasing curves were calculated with the aid of dedicated C++ programs. The idealized antiparallel structure with extended β-strands and the register given by a hydrogen bond between the amide of Ala-7 and the carbonyl of Leu-14 was defined as follows: distance between the ^{15}N and ^{13}C labels d_{NC} = 4.2 Å, periodicity d_{NN} = 9.6 Å within the sheet, and d_{NC} vector was perpendicular to the strand axis.

Results and Discussion

To stimulate the formation of a stable coiled coil (25–28), Ile and Leu residues were placed at the **a** and **d** positions of the two heptad repeats defining the consensus segment of this type of

Table 1. CD, urea denaturation, sedimentation equilibrium, Congo red staining, protofibril formation, hydropathy, and transition time data for ccβ variants

Peptides	$[\Theta]_{222}$,* 10^3 deg cm^2 dmol^{-1}	C_m,† M	MW,‡ kDa	CR§	PF¶	GRAVY‖	TT,** min
ccβ-p	−23.5	3.4	5.9	+	+	−0.38	4,100 (300)
ccβ-Met	−21.6	2.4	6.3	+	+	−0.49	65 (12)
ccβ-MetO	−19.2	1.5	6.2	−	−	ND	ND††

ND, not determined.

*$[\Theta]^{222}$ measured at 4°C at peptide concentrations (monomer) of 0.2 mg/ml.

†Midpoints of urea-induced equilibrium transitions determined at 4°C and at peptide concentrations (monomer) of 0.15 mg/ml. The error for each value is <10%.

‡Average molecular masses determined at 4°C and at peptide concentrations between 0.1 and 0.5 mg ml^{-1}. The error for each value is <10%. The sequence predicted average molecular masses of the peptides are 2.1 kDa for ccβ-p and 2.2 kDa for ccβ-Met and ccβ-MetO, respectively.

§Congo red staining of heat-induced fibril samples.

¶Formation of protofibrils verified by TEM.

‖Grand average hydropathy index scores (47).

**Transition time for fibril formation at 37°C and at peptide concentrations (monomer) of 0.2 mg/ml. The length of the lag phase is given in parentheses. The error for each value is <20%.

††No aggregate formation was observed for the ccβ-MetO derivative, even after incubation of a 20 mg/ml peptide solution for 72 h at 90°C or after attempts to seed the system by addition of preformed ccβ-Met fibrils.

fold (Fig. 1 *a* and *b*). In addition, Arg and Glu were incorporated at positions **b**, **c**, **e**, and **g** in a manner designed to permit optimal intra- and interhelical electrostatic interactions. The core sequence was flanked by N- and C-terminal acetylated Ser- and Gly-amidated capping residues (29), respectively. Importantly, this arrangement of residues is also compatible with the binary sequence patterning of stretches of hydrophobic and polar residues (ref. 30 and Fig. 1 *a* and *c*), which has been found to favor β-sheet and amyloid formation (31). Therefore, to complete the design of the parent peptide, referred to as ccβ-p, Ala and Leu residues were placed at the remaining **f** positions (residues denoted as X_7 and X_{14}).

The validity of the ccβ-p design was established by means of a variety of biophysical methods. The CD spectrum recorded from ccβ-p at 4°C confirmed the presence of substantial α-helical structure (Fig. 2*a*), and AUC studies indicated the formation of a trimer (Table 1). The stability of the helical trimeric complex formed by ccβ-p was probed by urea-induced unfolding monitored by CD at 222 nm (Fig. 2*b* and Table 1). The complex readily dissociated after addition of the denaturant and displayed a sigmoidal unfolding profile. The helical signal was fully regained after renaturation, demonstrating that the urea-induced unfolding process is reversible. The overall fold and topology of ccβ-p in its α-helical state was determined by x-ray crystallography at 2-Å resolution. As shown in Fig. 2*c*, the peptide forms a bundle of three parallel α-helices that coil slightly around each other in a left-handed manner. Consistent with the coiled-coil design, the Ile and Leu side chains occupying the hydrophobic **a** and **d** core positions are packed in a knobs-into-holes fashion, and the Arg-8 and Glu-13 side chains form a tight network of **g** to **e′** interhelical salt bridges. No intrahelical salt bridges are seen in the structure. The acetyl moiety of Ser-1 caps the helical monomer by forming an intrachain hydrogen bond with the N-terminal main-chain nitrogen atom. Together with the solution studies, these results are consistent with ccβ-p folding into a native-like α-helical coiled-coil structure at low temperatures (32).

The propensity of the ccβ-p coiled coil to undergo a conformational switch into a β-sheet-rich structure was assessed by CD at elevated temperatures. At 37°C and at a peptide concentration of 0.2 mg/ml, after an initial lag phase, the helical signal with minima at 208 and 222 nm transformed into one with a single minimum centered at 217 nm (Fig. 2*a*), which is consistent with the formation of β-sheet structures. The helical signal was not regained after cooling, indicating that the process of β-sheet formation is essentially irreversible. The length of the lag phase, as well as the slope of the growth phase, was both temperature- and concentration-dependent: At 50°C, the lag phase was shortened 15-fold and increasing the peptide concentration to 1 mg/ml reduced it by 3-fold at 37°C. Addition of preformed aggregates rich in β-sheet structure shortened the transition time by eliminating the lag phase, and also accelerating the growth rate (Fig. 2*d*). These findings are consistent with a nucleation-dependent self-assembly process for ccβ-p (9).

The structure of ccβ-p in its β-sheet-rich form was analyzed by a combination of complementary spectroscopic and microscopic techniques. As shown in Fig. 3*a Upper*, ccβ-p samples in PBS that were withdrawn during the early stages of assembly and were inspected by TEM, revealed a series of discrete prefibrillar structures. These structures are markedly similar to the protofibrillar aggregates reported for a wide range of disease- and nondisease-related proteins (5, 9, 33). TEM micrographs of mature ccβ-p samples reveal long fibrils of heterogeneous morphologies that appear as bundles made of single filaments 50–80 Å in diameter (Fig. 3*a Lower*). The addition of Congo red to samples containing fibrils produced the green birefringence under crosspolarized light, which is characteristic of amyloid structures (Table 1). TEM micrographs of mature samples obtained in water reveal single and frequently twisted fibrils with much more uniform morphology and with widths ranging from 40 to 80 Å (Fig. 3*b*). X-ray diffraction images obtained with the x-ray beam perpendicular to the major axis of the fibril (Fig. 3*c*) are consistent with a laminated cross-β-structure (7) with a sharp and intense 4.8-Å reflection on the meridian and more diffuse reflections at 11 and 22 Å on the equator. The two equatorial reflections are compatible with three or more β-sheets forming the core of the fibril structure (34). Fourier transform infrared spectra collected from fibrillar ccβ-p samples yielded one major band in the amide I region centered at 1,613 cm^{-1} and a minor one centered at 1,683 cm^{-1} (Fig. 3*d*), a pattern characteristic of antiparallel β-sheets. The absence of any other dominant bands in the spectra suggests that all ccβ-p residues adopt a predominantly extended β-sheet conformation.

High ionic strength and elevated temperatures both accelerated the rate of ccβ-p fibril formation (data not shown), indicating that hydrophobic interactions are likely to play an important role in their assembly. To test this hypothesis, a ccβ variant was prepared in which Met residues were placed at the heptad **f**7 and **f**14 positions (referred to as ccβ-Met; Fig. 1). Mutations of heptad **f** residues are not expected to interfere with the ccβ coiled-coil structure, because these positions do not participate in the formation of the hydrophobic core. Met was chosen

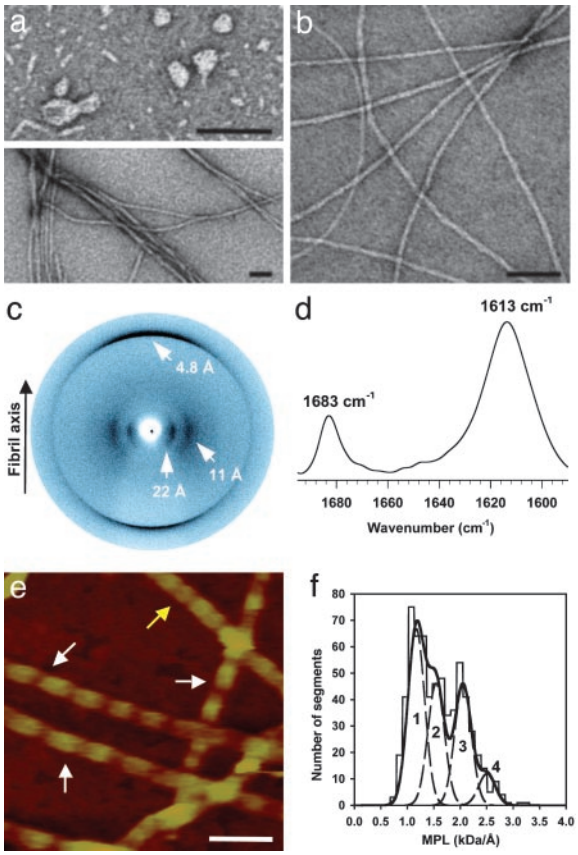

Fig. 3. Structural analysis of ccβ amyloid aggregates. (*a*) TEM micrograph of negatively stained ccβ-p protofibrillar intermediates (*Upper*) and mature ccβ-p fibrils (*Lower*) obtained in PBS. (*b*) TEM micrograph of negatively stained mature ccβ-p fibrils obtained in water. (*c*) X-ray diffraction image of ccβ-p fibrils obtained with the beam perpendicular to the fiber axis. (*d*) Fourier transform infrared spectrum in the amide I region recorded from ccβ-p fibrils. (*e*) ccβ-Met fibrils imaged by AFM in aqueous solution. The arrows indicate the two prominent fibril populations, which are characterized by 590 $\pm$ 50 Å (white arrows) and 300 $\pm$ 50 Å (yellow arrow) periodicities. (*f*) STEM-MPL histogram of unstained and freeze-dried ccβ-Met fibrils. The data could be fitted well by four Gaussian curves peaking at 1.17 (peak 1), 1.55 (peak 2), 2.06 (peak 3), and 2.51 kDa/Å (peak 4) with an SD for each peak of 0.16 kDa/Å. (Scale bars, 500 Å.)

because this residue does not show a dramatically different intrinsic propensity to favor either α-helix or β-sheet structures when compared with Ala or Leu (35), and does not substantially alter the overall hydrophobicity of the peptide (Table 1). In addition, it can be chemically oxidized to a polar sulfoxide group that is expected to disrupt the two short binary hydrophobic/polar sequence patterns present in the sequence (Fig. 1*c*); this form of the peptide is referred to as ccβ-MetO.

As expected, the formation of a coiled-coil structure is not affected by the substitutions, and the stabilities of the ccβ variants are comparable with that of the parent peptide (Fig. 2*b* and Table 1). Protofibrils and mature fibrils formed by ccβ-Met and inspected by TEM are visually indistinguishable from those obtained from ccβ-p. However, ccβ-Met fibril assembly was found to be $\approx$60 times faster than that of the parent peptide (Fig. 2 *d* and *e* and Table 1). In marked contrast to the aggregation behavior of ccβ and ccβ-Met, no aggregate formation was observed for the ccβ-MetO derivative even after incubation of a 20-mg/ml peptide solution for 72 h at 90°C or after attempts to seed the system by addition of preformed ccβ-Met fibrils. Thermal denaturation profiles recorded from ccβ-MetO by CD revealed fully reversible sigmoidal transitions with single inflection points (midpoint of the unfolding transition T_m = 46°C at 0.15 mg/ml; data not shown). Interestingly, ccβ-Met amyloid formation was slowed down by the presence of an equimolar amount of ccβ-p, although the lag phase was not affected (Fig. 2*e*). This finding suggests that the more slowly aggregating ccβ-p peptide influences the rate of ccβ-Met fibril growth by interfering with the packing of the peptide molecules within the fibrils. Consistent with this conclusion, the presence of an equimolar amount of ccβ-MetO resulted in strong suppression of amyloid fibril formation by ccβ-Met (Fig. 2*e*). These results support the hypothesis that interactions between hydrophobic side chains play a decisive role in the assembly of ccβ amyloid fibrils.

ccβ-Met fibrils obtained in water were further analyzed by AFM and STEM. Imaging of ccβ-Met fibrils in aqueous solution by AFM (Fig. 3*e*) revealed two prominent populations, characterized by axial repeats of 590 $\pm$ 50 (white arrows) and 300 $\pm$ 50 Å (yellow arrows), and maximum and minimum heights of 58 $\pm$ 5 and 36 $\pm$ 5 Å, and 74 $\pm$ 9 and 61 $\pm$ 8 Å, respectively. MPL measurements of ccβ-Met fibrils imaged by STEM indicated a minimum average MPL of 1.17 $\pm$ 0.16 kDa/Å and three higher values each at a mass increment of $\approx$0.4 kDa/Å (Fig. 3*f*). Assuming a cross-β conformation of extended strands with a calculated MPL of 2.1 kDa/4.8 Å = 0.438 kDa/Å for one cross-β lamina, these values indicate the presence of a heterogeneous population of fibrils, the major one consisting of segments of three β-sheets, and three additional ones consisting of four, five, and six sheets.

Based on the experimental data, we propose a structural model of the basic ccβ amyloid subunit. The model involves a laminated cross-β conformation of a minimum of three β-sheets in which individual β-strands are fully extended, and the number of hydrophobic contacts between the side chains of residues at positions 5/7/9 and 12/14/16 is maximized in both the intra- (Fig. 4*a*) and the intersheet (Fig. 4*b*) packing modes. As a result, the individual β-strands are arranged off-register and in an antiparallel fashion throughout the structure, allowing the formation of an extensive network of salt bridges between charged side chains. The minimum cross-section dimension of 62 $\times$ 33 Å and the corresponding MPL of 1.31 kDa/Å calculated for this ccβ fibril model are fully consistent with the structural data (Fig. 3). The proposed alignment and register within the β-sheet was further probed by solid-state NMR distance measurements on a sample of ccβ-p fibrils obtained at neutral pH and labeled selectively with ^{15}N at the amide position of Ala-7 and with ^{13}C at the carbonyl position of Leu-14. REDOR measurements of the coupling between these two nuclei provide support for an antiparallel out-of-register alignment of the constituent strands in which Ala-7 is hydrogen-bonded to Leu-14 (Fig. 4*c*). In addition, REDOR measurements carried out on a ccβ-p sample containing 12% labeled and 88% unlabeled peptide (Fig. 4*d*) excludes the possibility of intrachain hydrogen bonds between Ala-7 and Leu-14, and therefore support the existence of an extended conformation for the peptide molecules in the fibrillar structure.

For many model systems, a laminated cross-β structure has been proposed (7, 22, 34, 36). The model derived for ccβ shares many features characterizing this type of fold. For polyglutamine aggregates associated with Huntington's disease, models based on a β-helix fold have been put forward (37). However, both the length of the sequence as well as the ensemble of the data presented on the fibrillar form do not support such an alternative conformation for ccβ.

The detailed structural information presented for the ccβ model system in both its α-helical and β-sheet conformations provides a strong rational basis for a systematic dissection of the driving forces involved in amyloid formation and the evaluation

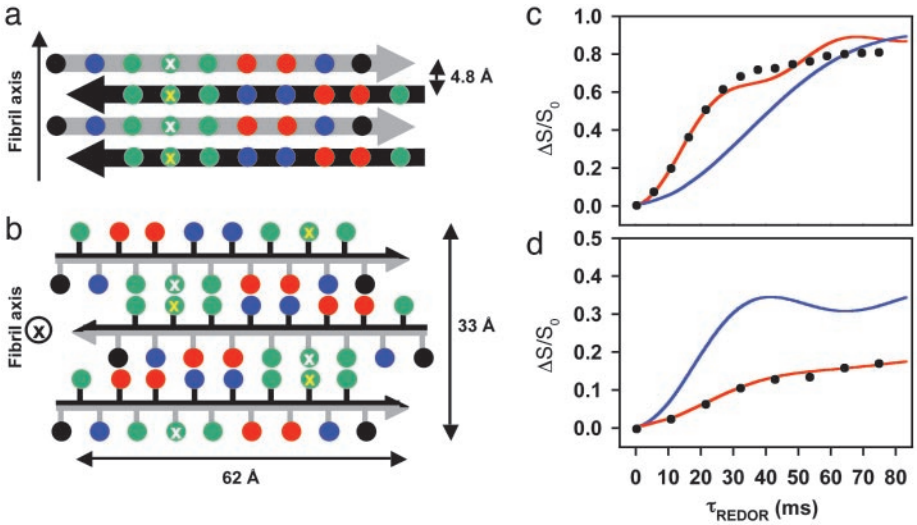

Fig. 4. Proposed ccβ fibril model. View of four β-strands perpendicular to the plane of the β-sheets (*a*) and of the fibril cross section (*b*). Adjacent strands are related by a twofold screw axis along (*a*) and perpendicular to (*b*) the long fibril axis. Amino acid side chains are represented as spheres; the color code is the same as in Fig. 1. The black and gray arrows discriminate between the two faces of the β-strand. Residues at positions 7 and 14 are marked by white and yellow crosses, respectively. (*c*) REDOR difference signal $\Delta S/S_0$ from a sample of ccβ fibrils with ^{15}N label at the amide nitrogen of Ala-7 and ^{13}C label at the carbonyl carbon of Leu-14 as a function of dephasing time τ_{REDOR}. Experimental REDOR difference data (●) were obtained from the peak intensities of the carbonyl resonance. The SD for each data point was ± 0.01. The red curve was calculated by assuming an idealized antiparallel structure with extended β-strands and the register being defined by a hydrogen bond between the amide of Ala-7 and the carbonyl of Leu-14. The agreement of the simulation to the data is excellent for the important short dephasing times <20 ms where the transfer is determined primarily by the shorter distance d_{NC}. The blue curve was calculated for a structure in which the register of the strands has been shifted by one residue. (*d*) REDOR measurements (●) on a 12% double-labeled fibrillized ccβ-p sample. The red and blue curves were calculated for extended interchain hydrogen-bonded β-strands and for a putative hairpin model with intrachain hydrogen bonds between the labeled residues, respectively.

of their relative importance. The destabilization of the native state after mutation is generally acknowledged to be a major factor in controlling amyloid formation by a globular protein (6, 38, 39). However, it has recently become apparent that many other factors also influence the process of aggregation and amyloid formation, including the kinetic barrier between the oligomeric and dissociated states, the nature of any residual structure present in the denatured state, the secondary structural propensities exhibited by the sequence, and the physicochemical properties of the polypeptide chain itself, such as charge or hydrophobicity (13, 36, 40–43). Perturbation of such factors due to the presence of a mutation or other causes, such as chemical modification of side chains as a result of protein misprocessing or aging, can therefore perturb the propensity of a given system to aggregate.

In this study, observation of the dramatic effect of the substitutions of Ala-7 and Leu-14 with Met and its sulfoxide derivative, in conjunction with the structural model, showing the close proximity of these residues (Fig. 4), provides strong evidence for the influence of a small number of site-specific hydrophobic interactions on the packing of the peptide molecules within the fibrils, and hence on the dynamics of amyloid formation. In particular, the observed increase in rate by a factor of 75 resulting from incorporation of the two Met residues compares with a factor of only 1.9 predicted for the effect of the two substitutions on the intrinsic propensity of ccβ-p to aggregate (43). This difference of a factor of 39 shows the additional effect of the specific packing interactions within the fibrillar structure in this system. The magnitude of this effect testifies to the success of the design strategy in which packing considerations were expected to play an important role. The fact that in natural polypeptide chains such interactions appear generally to be smaller in magnitude (43) supports the suggestion that many natural systems may select against sequences that are particularly favorable for stable amyloid structures (31).

This particular observation helps to rationalize a number of pathological conditions linked to specific hydrophobic mutations that have little effect on the overall stability of the protein or on the other features mentioned above (43, 44). In the light of the structural model, as the kinetics of amyloid formation in ccβ appear to be strongly influenced by specific hydrophobic packing interactions within the fibril, polymorphism at a critical site within a disease-associated amyloidogenic protein could represent an effective mechanism for delaying the onset of amyloid formation, not only by reducing the concentration of the homotypic species but also by slowing down the kinetics of the more rapidly aggregating species in the polymorphic mixture by interfering with its fibril packing. An important example of this point is sporadic Creutzfeldt–Jakob disease that occurs predominantly in individuals that are homozygous with respect to a common prion protein polymorphism at codon 129, resulting in either a Met or a Val residue (45). Our findings that a mixture of ccβ-p and ccβ-Met aggregates much more slowly than does either of these peptides in isolation suggest that a mismatch in hydrophobic interactions could explain the slower aggregation process in deposition diseases that afflict heterozygotic individuals (46).

The finding that all amyloid fibrils share some common characteristics such as fibril morphology and architecture offers the prospect that simple model systems can be used to systematically assess the factors that predispose a native protein to form amyloid fibrils. A significant difference to other *de novo*- and peptide-based model systems is that the designed ccβ precursor is protein-like. This is an important feature because it allows us to study the relationship between the stability of the native state of a protein and the factors underlying amyloid formation in a simplified manner. This approach in turn has an advantage over studies of natural sequences, where the complexity and size of the proteins often hinders a detailed rational approach to these processes. We believe, therefore, that the ccβ system provides an

exceptionally favorable platform from which to develop a more detailed understanding of the origin and progression of the increasing number of fatal human disorders associated with amyloid formation.

We thank Dr. R. Glockshuber for fruitful discussion; Drs. J. van Oostrum and U. Aebi for generous support; A. Lustig for assistance with the AUC experiments; V. Olivieri for STEM imaging; and the Interdisciplinary Center for Microscopy of the University of Basel for excellent assistance and rapid access to TEM. The STEM was supported by Swiss National Foundation and the Maurice E. Müller Foundation of Switzerland. R.A.K. is a Wellcome Trust Research Career Development Fellow. M.O.S. was supported by Novartis Pharma AG during the initial phase of this work. J.Z. and C.M.D. acknowledge support from a Wellcome Trust grant.

1. Taylor, J. P., Hardy, J. & Fischbeck, K. H. (2002) *Science* **296,** 1991–1995.
2. Hardy, J. & Selkoe, D. J. (2002) *Science* **297,** 353–356.
3. Guijarro, J. I., Sunde, M., Jones, J. A., Campbell, I. D. & Dobson, C. M. (1998) *Proc. Natl. Acad. Sci. USA* **95,** 4224–4228.
4. Fändrich, M., Fletcher, M. A. & Dobson, C. M. (2001) *Nature* **410,** 165–166.
5. Bucciantini, M., Giannoni, E., Chiti, F., Baroni, F., Formigli, L., Zurdo, J., Taddei, N., Ramponi, G., Dobson, C. M. & Stefani, M. (2002) *Nature* **416,** 507–511.
6. Kelly, J. W. (1996) *Curr. Opin. Struct. Biol.* **6,** 11–17.
7. Sunde, M., Serpell, L. C., Bartlam, M., Fraser, P. E., Pepys, M. B. & Blake, C. C. (1997) *J. Mol. Biol.* **273,** 729–739.
8. Cohen, F. E. & Prusiner, S. B. (1998) *Annu. Rev. Biochem.* **67,** 793–819.
9. Rochet, J.-C. & Lansbury, P. T., Jr. (2000) *Curr. Opin. Struct. Biol.* **10,** 60–68.
10. Dobson, C. M. (2002) *Nature* **418,** 729–730.
11. García-Echeverría, C. (1996) *Bioorg. Med. Chem. Lett.* **6,** 229–232.
12. Steinmetz, M. O., Stock, A., Schulthess, T., Landwehr, R., Lustig, A., Faix, J., Gerisch, G., Aebi, U. & Kammerer, R. A. (1998) *EMBO J.* **17,** 1883–1891.
13. Villegas, V., Zurdo, J., Filimonov, V. V., Aviles, F. X., Dobson, C. M. & Serrano, L. (2000) *Protein Sci.* **9,** 1700–1708.
14. Chiti, F., Webster, P., Taddei, N., Clark, A., Stefani, M., Ramponi, G. & Dobson, C. M. (1999) *Proc. Natl. Acad. Sci. USA* **96,** 3590–3594.
15. Müller, S. A., Goldie, K. N., Bürki, R., Häring, R. & Engel, A. (1992) *Ultramicroscopy* **46,** 317–334.
16. Goldsbury, C. S., Cooper, G. J., Goldie, K. N., Muller, S. A., Saafi, E. L., Gruijters, W. T., Misur, M. P., Engel, A., Aebi, U. & Kistler, J. (1997) *J. Struct. Biol.* **119,** 17–27.
17. Green, J., Goldsbury, C., Mini, T., Sunderji, S., Frey, P., Kistler, J., Cooper, G. & Aebi, U. (2003) *J. Mol. Biol.* **326,** 1147–1156.
18. Brünger, A. T., Adams, P. D., Clore, G. M., DeLano, W. L., Gros, P., Grosse-Kunstleve, R. W., Jiang, J.-S., Kuszewski, J., Nilges, M., Pannu, N. S., *et al.* (1998) *Acta Crystallogr. D* **54,** 905–921.
19. Gerber, P. R. & Müller, K. J. (1995) *J. Comput. Aided Mol. Des.* **9,** 251–268.
20. Bricogne, G. (1997) *Methods Enzymol.* **276,** 361–423.
21. Gullion, T. & Schaefer, J. (1989) *J. Magn. Reson.* **81,** 196–200.
22. Tycko, R. (2003) *Biochemistry* **42,** 3151–3159.
23. Jaroniec, C. P., MacPhee, C. E., Astrof, N. S., Dobson, C. M. & Griffin, R. G. (2002) *Proc. Natl. Acad. Sci. USA* **99,** 16748–16753.
24. Anderson, R. C., Gullion, T., Joers, J. M., Shapiro, M., Villhauer, E. B. & Weber, H. P. (1995) *J. Am. Chem. Soc.* **117,** 10546–10550.
25. Cohen, C. & Parry, D. A. D. (1990) *Proteins* **7,** 1–15.
26. Kohn, W. D. & Hodges, R. S. (1998) *Trends Biotechnol.* **16,** 379–389.
27. Kammerer, R. A., Schulthess, T., Landwehr, R., Lustig, A., Engel, J., Aebi, U. & Steinmetz, M. O. (1998) *Proc. Natl. Acad. Sci. USA* **95,** 13419–13424.
28. Burkhard, P., Meier, M. & Lustig, A. (2000) *Protein Sci.* **9,** 2294–2301.
29. Richardson, J. S. & Richardson, D. C. (1988) *Science* **240,** 1648–1652.
30. Takahashi, Y., Ueno, A. & Mihara, H. (2000) *Structure (London)* **8,** 915–925.
31. West, M. W., Wang, W., Patterson, J., Mancias, J. D., Beasley, J. R. & Hecht, M. H. (1999) *Proc. Natl. Acad. Sci. USA* **96,** 11211–11216.
32. Betz, S. F., Raleigh, D. P. & DeGrado, W. F. (1993) *Curr. Opin. Struct. Biol.* **3,** 601–610.
33. Walsh, D. M., Hartley, D. M., Kusumoto, Y., Fezoui, Y., Condron, M. M., Lomakin, A., Benedek, G. B., Selkoe, D. J. & Teplow, D. B. (1999) *J. Biol. Chem.* **274,** 25945–25952.
34. Blake, C. C., Serpell, L. C., Sunde, M., Sandgren, O. & Lundgren, E. A. (1996) *Ciba Found. Symp.* **199,** 6–15.
35. Munoz, V. & Serrano, L. (1994) *Proteins* **20,** 301–311.
36. Lopez De La Paz, M., Goldie, K., Zurdo, J., Lacroix, E., Dobson, C. M., Hoenger, A. & Serrano, L. (2002) *Proc. Natl. Acad. Sci. USA* **99,** 16052–16057.
37. Perutz, M. F., Finch, J. T., Berriman, J. & Lesk, A. (2002) *Proc. Natl. Acad. Sci. USA* **99,** 5591–5595.
38. Booth, D. R., Sunde, M., Bellotti, V., Robinson, C. V., Hutchinson, W. L., Fraser, P. E., Hawkins, P. N., Dobson, C. M., Radford, S. E., Blake, C. C. & Pepys, M. B. (1997) *Nature* **385,** 787–793.
39. Ramirez-Alvarado, M., Merkel, J. S. & Regan, L. A. (2000) *Proc. Natl. Acad. Sci. USA* **97,** 8979–8984.
40. Nielsen, L., Frokjaer, S., Brange, J., Uversky, V. N. & Fink, A. L. (2001) *Biochemistry* **40,** 8397–8409.
41. Chiti, F., Taddei, N., Baroni, F., Capanni, C., Stefani, M., Ramponi, G. & Dobson, C. M. (2002) *Nat. Struct. Biol.* **9,** 137–143.
42. Hammarström, P., Schneider, F. & Kelly, J. W. (2001) *Science* **293,** 2459–2462.
43. Chiti, F., Stefani, M., Taddei, N., Ramponi, G. & Dobson, C. M. (2003) *Nature* **424,** 805–808.
44. Liemann, S. & Glockshuber, R. (1999) *Biochemistry* **38,** 3258–3267.
45. Mead, S., Stumpf, M. P., Whitfield, J., Beck, J. A., Poulter, M., Campbell, T., Uphill, J. B., Goldstein, D., Alpers, M., Fisher, E. M. & Collinge, J. (2003) *Science* **300,** 640–643.
46. Come, J. H. & Lansbury, P. T., Jr. (1994) *J. Am. Chem. Soc.* **116,** 4109–4110.
47. Kyte, J. & Doolittle, R. F. (1982) *J. Mol. Biol.* **157,** 105–132.